JP1.14   A PREFERRED SCALE FOR WARM CORE INSTABILITY IN A NON-CONVECTIVE MOIST BASIC STATE

Brian H. Kahn

Jet Propulsion Laboratory, California Institute of Technology, Pasadena, CA

Douglas M. Sinton[*]

Department of Meteorology, San José State University, San José, CA

ABSTRACT

The existence, scale, and growth rates of sub-synoptic scale warm core circulations are investigated with a simple parameterization for latent heat release in a non-convective basic state using a linear two-layer shallow water model. For a range of baroclinic flows from moderate to high Richardson number, conditionally stable lapse rates approaching saturated adiabats consistently yield the most unstable modes with a warm-core structure and a Rossby number $\sim O(1)$ with higher Rossby numbers stabilized. This compares to the corresponding most unstable modes for the dry cases which have cold-core structures and Rossby numbers $\sim O(10^{-1})$ or in the quasi-geostrophic range. The maximum growth rates of 0.45 of the Coriolis parameter are an order of magnitude greater than those for the corresponding most unstable dry modes. Since the Rossby number of the most unstable mode for nearly saturated conditions is virtually independent of Richardson number, the preferred scale of these warm core modes varies directly with the mean vertical shear for a given static stability.

This scale relation suggests that the requirement to maintain nearly saturated conditions on horizontal scales sufficient for development can be met more easily on the preferred sub-synoptic horizontal scales associated with weak vertical shear. Conversely, the lack of instability for higher Rossby numbers implies that stronger vertical shears stabilize smaller, sub-synoptic regions which are destabilized for weaker vertical shears. This has implications for the scale and existence of warm core circulations in the tropics such as those assumed *a priori* in WISHE.

---

[*] *Corresponding author address:* Douglas M. Sinton, Dept. of Meteorology, San José State University, One Washington Square, San José, CA 95192-0104: e-mail: sinton@met.sjsu.edu

1. INTRODUCTION

Tropical cyclones, mesoscale convective systems (MCS), and polar lows require moisture supplied by warm core, sub-synoptic-scale circulations that develop in generally saturated, near neutral conditions over a range of weak to moderate vertical shears (Xu and Emanuel 1989; Emanuel 1989; Houze 2004). Accounting for the scale of such warm core circulations has proven to be elusive. In a recent paper on the relationship between extra-tropical precursors and ensuing tropical depressions, Davis and Bosart (2006) state:

> "No theory exists that accurately describes the scale contraction from the precursor disturbance (1000 – 3000 km) to the developing depression (100 – 300 km)."

This provides the primary motivation for this study: to determine if there is a preferred scale for warm core instability similar to the scale of the warm core circulations that supply moisture to tropical cyclones.

When embarking on a linear instability study, it is important to consider how such studies apply to real atmospheric phenomena (e.g. Descamps et al. 2007) given their inappropriateness for all but the most primitive simulations where there is no interaction between the perturbation and the basic state. Furthermore, Descamps et al. (2007) conclude that linear scales only broadly agree with those of real phenomena. Any consideration of convection interacting with larger scales is clearly not appropriate for a linear study and correspondingly, the current investigation is limited to a non-convective basic state. Nevertheless, if it can be shown that a preferred scale for warm core instability exists, its sensitivity to basic state parameters such as baroclinity and saturation may shed some light on the aforementioned scale gap described by Davis and Bosart (2006).

A review of previous efforts to find a preferred scale for warm core instability reveals the problems associated with the disparity between the convective scale and larger scales. Earlier investigations into the scale of warm core phenomena focused on the

interaction of cumulus scale convection with the larger scale circulation that is required to converge the moisture that sustains the convection. These types of investigations are commonly described as conditional instability of the second kind (CISK). Because the cumulus scale is a preferred scale for convective instability arising from the conversion of CAPE and downward available potential energy (DAPE), CISK has yet to provide a satisfactory explanation for the observed, sub-synoptic scale as the only preferred scale for instability with a finite growth rate (Charney and Eliassen 1964; Mak 1981; Fraedrich and McBride 1995).

Given that the latent heating in CISK redistributes moist entropy without generating it (Xu and Emanuel 1989; Arakawa 2004), some of the more recent studies of warm core, sub synoptic-scale phenomena have taken a finite amplitude approach that shifts the focus from convective heating as a source of instability to the issue of how the required moist static energy is supplied while assuming *a priori* the existence of a suitably scaled circulation to converge it (Emanuel 1986; Holton 2004). Wind induced surface heat exchange (WISHE) has emerged as an efficient process for injecting the required amounts of moist static energy to sustain convection in tropical cyclones and polar lows (Craig and Gray 1996). In a recent simulation (Montgomery et al. 2006), a pre-existing midlevel cyclonic mesoscale convective vortex (MCV) was needed in order to provide a suitable environment for organizing convection leading to tropical cyclogenesis.

A recent study of the role of tropical waves in tropical cyclogenesis (Frank and Roundy, 2006) found that a dominant baroclinic first internal mode structure is common to tropical waves near the genesis of tropical cyclones. Previous investigations into the effect of latent heat release on baroclinic instability using quasi-geostrophic models (Tokioka 1973; Mak 1982, 1983; Bannon 1986; Wang and Barcilon 1986; Thorncroft and Hoskins 1990) have shown moderate decreases in preferred scale and corresponding increases in growth rate (see Fig. 1 in Mak 1982) compared to the dry case along with modest increases in upshear phase tilt with height (see Fig. 4 in Mak 1982). There are, however, two limitations to the quasi-geostrophic approach to warm core, sub-synoptic-scale phenomena. First, the assumption of near geostrophy may not apply for sub-synoptic scales especially when the Rossby number (Ro) exceeds $O(10^{-1})$ (Moorthi and Arakawa 1985; Thorpe and Emanuel 1985) and the growth rate approaches the Coriolis parameter, f (Fraedrich and McBride 1995). Second, warm core systems are equivalently barotropic because the thickness and mass fields align as vertically-stacked structures. The resulting lack of thickness advection by the geostrophic wind prevents any conversion of zonal available potential energy (P_M) to eddy available potential energy (P_E) by the geostrophic wind thus precluding any quasi-geostrophic baroclinic instability for warm core systems. It is thus unsurprising that previous studies that used quasi-geostrophic formulations modified by latent heating parameterizations have been unsuccessful in accounting for the spectrum of observed sub-synoptic scale warm core structures.

A two layer shallow water model on an *f*-plane is one of the simplest models that is capable of both producing the baroclinic first internal mode discussed in Frank and Roundy (2006) while also resolving ageostrophic flows precluded by quasi-geostrophic limitations. Its simplicity and versatility make it a valuable tool for finding instabilities that might underlie some of the circulations, such as those assumed *a priori* in WISHE, that serve as catalysts for the recent advances in warm core numerical simulations. In this spirit, the motivation for the current investigation is to: (1) determine if there is an instability underlying the origin of warm core circulations that act as precursors to tropical cyclones; (2) assess the sensitivity of the growth rate and spatial scale to basic state parameters; and (3) determine whether the structure of such circulations might serve to converge water vapor as assumed *a priori* in WISHE, Montgomery et al. (2006), and in other works. The existence of such an instability may shed some light on factors affecting the origin, development, and scale of circulations, which heretofore have been initially prescribed to function as precursors for tropical cyclogenesis as in a recent zero vertical shear simulation by Nolan et al. (2007).

Accordingly, the current investigation uses the two-layer shallow water model from Orlanski (1968; henceforth IFW) and Sinton and Heise (1993) modified by a simple parameterization for latent heating. Section 2 describes the model configuration and physics, the latent heat parameterization, and model energetics. Section 3 examines the model solutions: a moist but non-convective mode with a warm core structure and a convergent circulation, with enhanced growth rates on a preferred scale determined by the magnitudes of vertical shear and saturation. Finally, Section 4 summarizes the characteristics of the non-convective moist mode and then examines the implications of the mode's existence and its scale dependence on vertical shear strength and saturation.

2. METHODOLOGY

2.1 Latent heating parameterization

The fluid interface in the two-layer shallow water model that separates two fluid layers with different densities (see Fig. 1) is analogous to an isentropic surface in a stably stratified atmosphere (e.g. Andrews et al. 1987). Latent heating due to vertical motion occurs as a mass exchange across isentropic surfaces. To emulate this in the shallow water system, the continuity equation in Sinton and Heise (1993) for each layer is modified by addition of the scalar *q*,
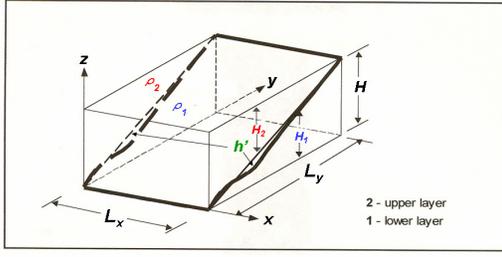
FIG. 1 Two layer shallow water model schematic. Thin solid and dashed lines represent $\overline{h}$ and $\rho_1 > \rho_2$

which multiplies each divergence term:

$$\frac{\partial h_m^{'}}{\partial t} = -\left(\begin{array}{l} U_m \dfrac{\partial h_m^{'}}{\partial x} + v_m^{'} \dfrac{dH_m}{dy} \\[2mm] + H_m(1-q)\nabla \bullet \mathbf{v_m^{'}} \\[2mm] + H_n q \nabla \bullet \mathbf{v_n^{'}} \end{array} \right)_{n \neq m} \quad (1)$$

with $h_1^{'} = h^{'}$, $h_2^{'} = H - h^{'}$, $H_1 = \overline{h}$, and $H_2 = H - \overline{h}$, and vertical layers: m = 1, 2; n = 2, 1, respectively (see Fig. 1). The effect of q is to modify the change in interface height, $h^{'}$, and mean column density, $\overline{\rho}$, by moving fluid across the interface (see Fig. 2). The latent heating is reversible as opposed to pseudoadiabtic as there is no partitioning between rising and subsiding motion. For $q = 0.5$ the mean column density is unchanged regardless of divergence (vertical velocity). As is shown later, $q = 0.5$ is the convective threshold. An examination of eqn (1) in the context of mass conservation demonstrates this. Conservation of mass requires on average:

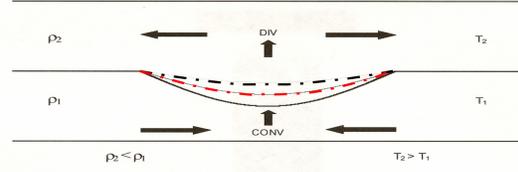$$H_1 \nabla \bullet \mathbf{v_1^{'}} = -H_2 \nabla \bullet \mathbf{v_2^{'}} \quad (2)$$

FIG. 2 Behavior of the fluid interface in the two-layer model. The depressed interface in the center of the figure represents a vertical column of less dense (warmer) fluid, relative to the neighboring fluid columns. The black dashed-dotted line is the height of the interface after vertical motion with no latent heating ($q = 0$), while the red dashed-dotted line is the height of the interface after model latent heating ($0 < q < 0.5$) moves some fluid from the lower layer to the upper layer.

Substituting eqn (2) into the continuity eqn (1) gives:

$$\frac{\partial h_1^{'}}{\partial t} = -H_1 \nabla \bullet \mathbf{v_1^{'}}(1-2q) - (U_1 \frac{\partial h_1^{'}}{\partial x} + v_1^{'} \frac{dH_1}{dy}) \quad (3)$$

and:

$$\frac{\partial h_2^{'}}{\partial t} = H_1 \nabla \bullet \mathbf{v_1^{'}}(1-2q) - (U_2 \frac{\partial h_2^{'}}{\partial x} + v_2^{'} \frac{dH_2}{dy}). \quad (4)$$

Thus, for the convective threshold of $q = 0.5$, divergence cannot affect the fluid interface (see Fig. 3) as the divergence terms in eqn (3) and eqn (4) vanish. The convective threshold case of $q = 0.5$ represents an atmosphere with a saturated adiabatic lapse rate as parcels move vertically without changing the density (temperature) of the fluid (atmospheric) column. For $q < 0.5$ the familiar cooling (warming) associated with rising (sinking) motion occurs as latent heating effects are less than adiabatic effects. For $q > 0.5$ the fluid column density decreases (increases) for rising (sinking) motion, reflecting the conversion of CAPE (DAPE) to sensible heat in a conditionally unstable atmosphere. The $q > 0.5$ case thus represents a convective basic state, and it is therefore not an appropriate case for this study given the results of the previous linear perturbation analyses discussed in the Introduction. In view of this, $q = 0.5$ is referred to as the convective threshold. Derivation of the model energetics confirms this behavior, and is detailed in the following sub-section.

3

$$\frac{dh'}{dt} = w_2' - q(w_1' + w_2') \; . \qquad (8)$$
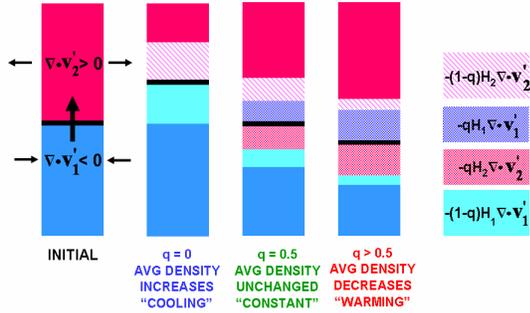
From eqn (6) in Mechoso and Sinton (1983):

$$\frac{dP_E}{dt} = g(\rho_1 - \rho_2)\int_0^{L_y}\left\langle \frac{dh'^2}{dt}\right\rangle dy \; . \qquad (9)$$

The limits of integration at $y = 0$ and $y = L_y$ can be substituted for $\pm\infty$ since the interface perturbation is confined to the region $0 \leq y \leq L_y$; $\langle \; \rangle$ represents an integration over the region $0 \leq x \leq L_x$, and g is gravity. First, define the generation of P_E by latent heating, W_Q as:

$$W_Q \equiv -g(\rho_1 - \rho_2)q\int_0^{L_y}\left\langle h'(w_1' + w_2')\right\rangle dy \; , \quad (10)$$

then integrate $[g\rho_1 h'\cdot(7) - g\rho_2 h'\cdot(8)]$, and lastly, apply the energy block diagram from Fig. 3 in Mechoso and Sinton (1983). Eqn (9) then becomes:

$$\frac{dP_E}{dt} = W_3 - (W_5 + W_3 - W_4) + W_Q \; , \qquad (11)$$

where the baroclinic conversion, W_3, the cross-isobaric conversion, W_5, and W_4, which is discussed in more detail following eqn (18), are defined by IFW (9.19), (9.20), and (9.21), respectively. Defining W_K as:

$$W_K \equiv W_5 + W_3 - W_4 \; , \qquad (12)$$

and applying IFW (9.29), the following relation for the conversion of P_E to K_E is obtained:

$$W_K = -g(\rho_1 - \rho_2)\int_0^{L_y}\left\langle h'\left(\frac{w_1' + w_2'}{2}\right)\right\rangle dy \; . \quad (13)$$

Comparison of eqn (10) and eqn (13) reveals that:

$$W_Q = 2qW_K \; . \qquad (14)$$

Define the baroclinic conversion as:

$$W_{BC} \equiv W_3 \; , \qquad (15)$$

FIG. 3 Latent heating cases for rising motion. Thick black line is interface separating denser fluid from less dense fluid. Solid red (blue) shading represents unaffected less (more) dense upper (lower) layer fluid. Pink diagonal shading represents less dense fluid removed from upper layer due to upper layer divergence $[-(1-q)H_2\nabla\cdot\mathbf{v_2'}]$. Blue textured pattern represents less dense fluid added to upper layer by mass exchange due to lower layer convergence $[-qH_1\nabla\cdot\mathbf{v_1'}]$. Red textured pattern represents denser fluid removed from lower layer by mass exchange due to upper layer divergence $[-qH_2\nabla\cdot\mathbf{v_2'}]$. Solid light blue shading represents denser fluid added to lower layer due to lower layer convergence $[-(1-q)H_1\nabla\cdot\mathbf{v_1'}]$.

2.2 Energetics

Using $h_1' = h'$; $h_2' = H - h'$, along with the relations

$$w_1' = -H_1\nabla\cdot\mathbf{v_1'} \; , \qquad (5)$$

and:

$$w_2' = H_2\nabla\cdot\mathbf{v_2'} \; , \qquad (6)$$

eqn (1) can be rewritten as:

$$\frac{dh'}{dt} = w_1' - q(w_1' + w_2') \qquad (7)$$

and:

4

and substitute eqn (13) into eqn (11) to obtain:

$$\frac{dP_E}{dt} = W_{BC} + W_Q - W_K \,. \qquad (16)$$

By substituting eqn (14) into eqn (16), the barotropic case, $W_{BC} = 0$, becomes:

$$\frac{dP_E}{dt} = W_K(2q-1) \,. \qquad (17)$$

Analogous to Fraedrich and McBride (1995), their ratio of diabatic heating to adiabatic cooling, γ, is defined here as $2q$. Eqn (17) shows that for the convective regime $q > 0.5$ ($\gamma > 1$), a direct circulation ($W_K > 0$) increases P_E as CAPE (DAPE) is converted to sensible heat at a greater rate than P_E is consumed by adiabatic cooling (heating). With this in mind, the model energetics can be represented by the four cases shown in Fig. 4. Cases (a) and (b) are dry cases ($q = W_Q = 0$). Case (a) is the standard dry baroclinic conversion cycle where $W_{BC} > W_K$ and Ro $\sim O(10^{-1})$ with Ro $= (U_2 - U_1)k/(2f)$ and $k = 2\pi/L_x$. Case (b) is the short-wave cutoff for dry baroclinic instability where $W_{BC} = W_K$ and Ro $\geq O(10^{-1})$. Case (c) is the convective case described above where $q > 0.5$ exceeds the convective threshold, and $W_Q > W_K$, thus precluding the need for W_{BC}. The preferred scale for instability is Ro $\sim O(\infty)$, or the cumulus scale. This is widely known as the "ultraviolet catastrophe", where the most unstable scale is the smallest (e.g. Majda and Shefter 2001). Accordingly, the convective case is not considered in the current investigation.

The focus of the current investigation is the non-convective case (d) where W_K is slightly larger than W_Q: $(W_K - W_Q)/|W_K| \ll 1$. This case is defined by an atmosphere approaching a saturated adiabatic lapse rate ($0.45 < q < 0.5$) with just enough baroclinic conversion [$W_{BC}/|W_K| \ll 1$ and $W_{BC} > (W_K - W_Q)$] so that $dP_E/dt > 0$. This can be compared to the case McBride and Fraedrich (1995) refer to as "fast mode without CISK mode" for $\gamma < 1$ (see McBride and Fraedrich 1995 Table 1), which is stable due to axisymmetry and absence of convection, but unstable in the shallow water model due to baroclinity. Substitution of the geostrophic meridional wind, defined as:

$$v'_{gm} = \left(\frac{1}{f \rho_m}\right) \frac{\partial p'_m}{\partial x} \qquad (18)$$

for the meridional wind, v'_m, in the definition for W_{BC} from IFW (9.19) reveals that the geostrophic component of W_{BC} is W_4 (IFW 9.20), henceforth referred to as the geostrophic baroclinic conversion W_{BCG}. The ageostrophic component of W_{BC} can then be defined as $W_{BC} - W_{BCG}$, henceforth W_{BCAG}, the ageostrophic baroclinic conversion. Due to the equivalent barotropy discussed earlier, warm core systems have $|W_{BCG} / W_{BCAG}| \ll 1$.
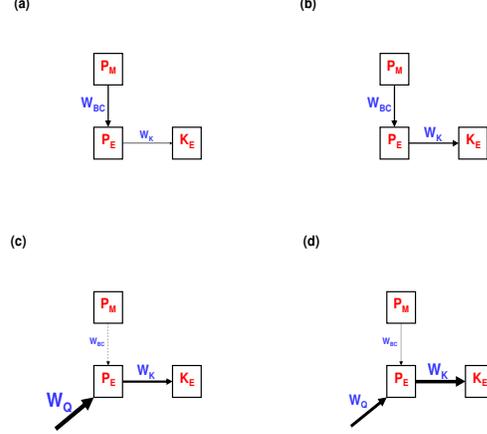

FIG. 4 Energetics for the cases: (a) $q = 0$; Ro $\sim O(10^{-1})$; (b) $q = 0$; Ro $\geq O(10^{-1})$; (c) $q > 0.5$; Ro $\sim O(\infty)$; (d) $0.45 < q < 0.5$; Ro $\sim O(1)$. Font size and arrow shaft thickness for energy conversions are proportional to their relative magnitudes. Dashed W_{BC} arrow shaft in (c) indicates W_{BC} is not required in this case.

In the case where the most unstable mode has a purely warm core structure, W_{BC} consists entirely of W_{BCAG}, thus precluding a warm core structure from occurring in a quasi-geostrophic system. Solutions of the current investigation show that this occurs for Ro $\sim O(1)$.

2.3 *Method of solution*

The method of solution is similar to Sinton and Heise (1993) but with the boundary conditions from IFW applied at $y = 0$; L_y. Eigenvalues and eigenvectors for the resulting system are found using an $N \times N$ coefficient matrix with $N = 2112$, which was the resolution needed to resolve modes for the highest Ri case for Ri $= [gH(\rho_1 - \rho_2)]/[\bar{\rho}(U_2 - U_1)^2]$. ($N > 2112$ overtaxed the software used to find eigenvectors.) For a fixed stratification, $g(\rho_1 - \rho_2)/(\bar{\rho}H)$, L_y varies as Ri$^{1/2}/f$. Thus L_y becomes large relative to the meridional scale of the perturbation for large Ri (Ri $> 10^3$). All eigenvalues are confirmed (see Appendix B in Sinton and Heise 1993) using the Newton-Raphson iteration method modified for q (see the Appendix). Note that unlike Sinton and Heise (1993), $dU_m/dy = 0$ in all cases so the effects of horizontal wind shear are not considered in this investigation.

3. RESULTS

3.1 Energy vectors

In order to minimize the influence of latent heating in the frontal regions where the interface intersects the upper and lower boundaries, a sinusoidal q profile (see Fig. 5) is used in all cases with q_c representing the maximum value of q, which occurs in the center of the meridional (y) domain where the interface is at midlevel.
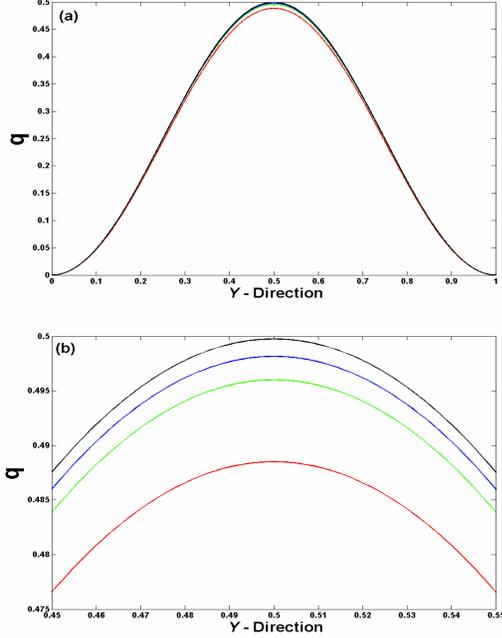

FIG. 5 Variation of q in y direction for various Ri's: a) over full domain; b) in center of domain for Ri: 10: red; 40: green; 100: blue; 1000: black.
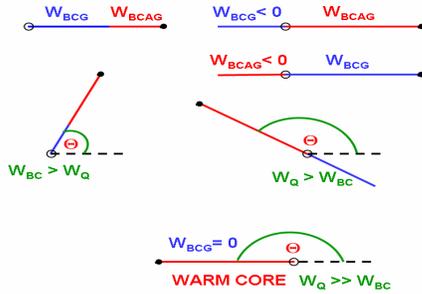

FIG. 6 Energy vector schematic with Θ as defined by eqn (19). The geostrophic component of W_{BC}, W_{BCG}, is the blue segment while the ageostrophic component of W_{BC}, W_{BCAG}, is the red segment of the vector shaft. The solid circle is the tip of the vector. Shaft segments between the open circle and tip represent positive values of W_{BCG} and/or W_{BCAG} while shaft segments on the opposite side of the open circle from the tip represent negative values of W_{BCG} and/or W_{BCAG}. W_{BCG} and W_{BCAG} are normalized by W_{BC} such that (W_{BCG} + W_{BCAG})/W_{BC} = 1. A warm core structure appears as a pure red vector pointing to the left (toward lower Ro on subsequent figures).

Energy vectors are defined by:

$$\Theta = \tan^{-1}\left(\frac{2W_Q}{W_{BC}}\right)$$

(19)

illustrated in Fig. 6, and they rotate to the left as the effect of latent heating increases, pointing vertically when $W_Q = W_{BC}$ and then into the second quadrant as $W_Q > W_{BC}$. Additionally, the phase lag between p_2' and p_1' corresponds to the sign of W_{BCG}. When W_{BCG} = 0, only W_{BCAG}, contributes to W_{BC} corresponding to a warm core structure with a 180° phase lag between p_2' and p_1'. Negative values of W_{BCG} correspond to a damping quasi-geostrophic configuration associated with a down shear phase lag > 180° between p_2' and p_1'.

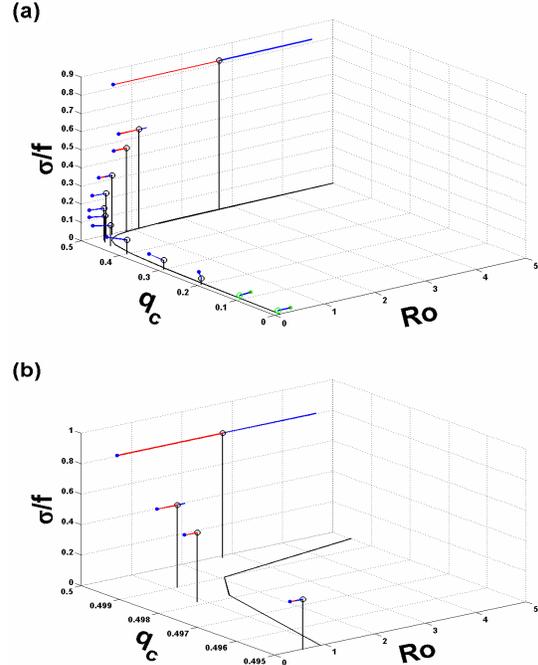**3.2 Sensitivity to variation of latent heating**

FIG. 7 Growth rate of most unstable mode normalized by f as a function of the maximum value of q in the center of the Y domain, q_c, and Ro for Ri 100. Energy vectors as in Fig. 6 and text. Thick solid line: Ro$_{CUT}$. Black stems and blue vector tips: E modes; green stems and vector tips: B modes. (b) Close up for $0.495 \leq q_c \leq$ 0.4999. Warm core mode: q_c = 0.49815.

6

Fig. 7 shows the growth rate, σ, normalized by f for the most unstable mode found for Ri = 100 as a function of Ro and q_c. There is a marked increase in both σ/f and Ro as q_c increases in the non-convective range beyond 0.45 but below the convective threshold of 0.5. Nevertheless, in this range instabilities only exist for Ro less than the values denoted by the thick solid line, denoting the short-wave cutoff, Ro$_{CUT}$, and its associated length scale:

$$L_{CUT} \cong \frac{U_2 - U_1}{f\,\mathrm{Ro}_{CUT}} \quad (20)$$

for $q_c < 0.5$, the non-convective regime. The warm core case with its pure red energy vector (see Fig. 7b) occurs for Ro = 0.883 and q_c = 0.49815. For values of Ro > 0.883 there is an increasing down shear phase lag > 180° between $p_2^{'}$ and $p_1^{'}$ associated with larger negative values of W_{BCG} as Ro increases. Finally, in Fig. 7a, the frontal (green stem) B modes (e.g. IFW; Sinton and Heise 1993; Sinton and Mechoso 1984) are most unstable for $q_c < 0.2$ while the zero phase speed and non-frontal (black stem) E modes (e.g. IFW; Mechoso and Sinton 1993; Sinton and Mechoso 1984) are most unstable for $0.2 \leq q_c < 0.5$ as the effect of latent heating in the interior overcomes frontal effects.
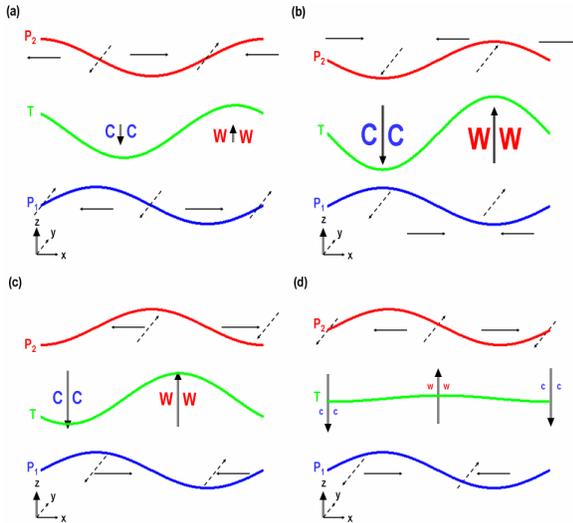

FIG. 8 Schematic of the four phase lags and associated circulations found for the (a) Ro $O(10^{-1})$; (b) Ro $O(1)$; (c) Ro $O(>1)$; (d) Ro $O(\gg 1)$ cases. Vertical arrow lengths are proportional to strength of vertical velocities. Font size for C's (cold) and W's (warm) proportional to amplitude of interface (thickness) perturbation. Solid arrows perturbation zonal velocity; dashed arrows perturbation meridional velocity.

Fig. 8 is a schematic of the phase lags and circulations for various Ro regimes. Scaling as in Sinton

(1984), the non-dimensional zonal momentum equation becomes:

$$\mathrm{Ro}\tilde{\sigma}\frac{\partial \tilde{u}_m^{'}}{\partial \tilde{t}} = -\left(\begin{array}{l} \mathrm{Ro}\tilde{U}_m\dfrac{\partial \tilde{u}_m^{'}}{\partial \tilde{x}} - \tilde{v}_m^{'} \\[2mm] + \mathrm{RiRo}\dfrac{\partial \tilde{p}_m^{'}}{\partial \tilde{x}} \end{array} \right)_{m=1,2} , \quad (21)$$

where the ~ overbar denotes non-dimensional variables. As Ro increases beyond 1, there is a stronger positive (negative) correlation between u' and p' in the lower (upper) layer due to the opposite sign of U_m in each layer. The corresponding divergence pattern associated with $\partial u'/\partial x$ in each layer aligns $p_2^{'}$ and $p_1^{'}$ (see Fig. 8d) consistent with the correlation between u' and p' in each layer.

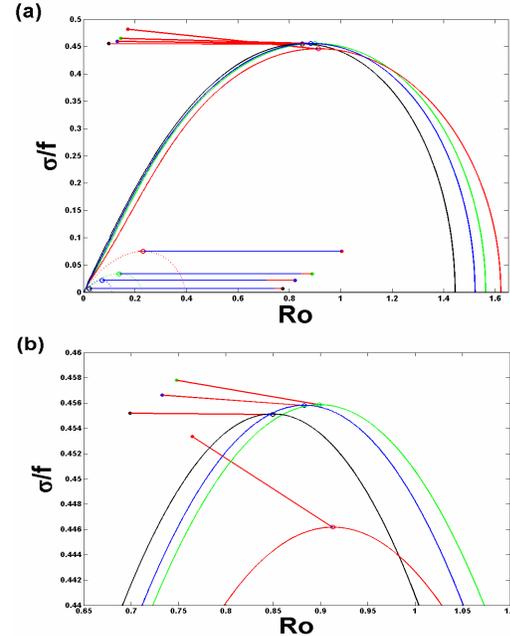### 3.3 Sensitivity to baroclinity for dry and moist cases

FIG. 9 Growth rates normalized by f vs Ro for the dry mode ($q_c = 0$; dotted) and warm core as most unstable mode (solid) for Ri 10 red (q_c 0.4885); Ri 40 (q_c 0.496) green; Ri 100 (q_c 0.49815) blue; Ri 1000 black (q_c 0.49976). Energy vectors as in Fig. 6. (b) Close-up of warm core as most unstable mode; notation same as in (a).

Fig. 9 shows the growth rates versus Ro for both the dry case ($q_c = 0$) and the case where the warm core structure is the most unstable mode for the four Ri's at 10, 40, 100, and 1000. A unique, non-zero q_c is determined for each Ri by varying q_c until the most unstable mode for each Ri has $W_{BCG} = 0$ over the domain, which corresponds to an average 180° phase

lag between $p_2^{'}$ and $p_1^{'}$. Since the Ri's have a constant density differential $(\rho_1 - \rho_2)/\overline{\rho} = 0.04$, the mean vertical shear $(U_2 - U_1)$ varies as $Ri^{-1/2}$.

The dry cases show the expected Ro ~ $Ri^{-1/2}$ (e.g. Simmons 1974) relationship for the most unstable baroclinic mode whose length scale is the Rossby radius of deformation, $L_o = \sqrt{\dfrac{gH(\rho_1 - \rho_2)}{\overline{\rho} f^2}}$. As q_c increases toward the convective threshold of 0.5, the effective static stability, $\dfrac{g(\rho_1 - \rho_2)(1 - 2q_c)}{\overline{\rho} H}$, the corresponding effective Ri, $Ri^* = (1 - 2q_c)Ri$, and the effective Rossby radius of deformation, $L_o^* = \sqrt{\dfrac{gH(\rho_1 - \rho_2)(1 - 2q_c)}{\overline{\rho} f^2}}$ all approach 0. The reduction in perturbation length scale is consistent with the reduction for quasi-geostrophic baroclinic instability in a moist basic state as effective static stability decreases for increased latent heating.

For the warm core as most unstable mode, Ri^* remains near 1 as q_c approaches 0.5 for increasing Ri. This accounts for Ro remaining near 1 despite $Ri^{-1/2}$ changing by an order of magnitude. Assuming the perturbation's meridional scale is comparable to its zonal scale, an effective Burger number can be defined analogously to Sinton and Heise (1993) (3.11):

$$Ro_{WC} \cong (2Ri^*)^{-1/2} \qquad (22)$$

where $Ro_{WC} \equiv$ Ro for the warm core as most unstable mode. Since $Ro_{WC} \sim O(1)$, its preferred length scale becomes:

$$L_{WC} \cong \left(\frac{U_2 - U_1}{f} \right). \qquad (23)$$

Compensating for the decrease in baroclinity as Ri increases, q_c increases slightly with Ri toward the 0.5 convective threshold. Despite this slight increase, q_c in all cases is confined to $0.4885 \leq q_c < 0.5$ indicating that the warm core instability as the preferred scale is limited to the non-convective regime of saturated nearly adiabatic lapse rates for Ri $\geq$ 10. As Ri increases, the energy vector angles (Fig. 9b) rotate toward 180° confirming that as baroclinity decreases an ever larger share of P_E comes from latent heating as opposed to baroclinity ($W_Q \gg W_{BC}$). This decouples Ro from its dry baroclinic $Ri^{-1/2}$ dependence.
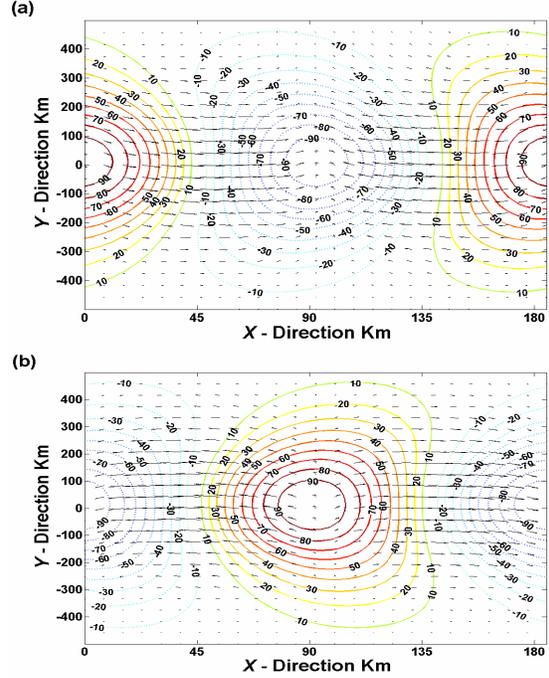
3.4 Warm core mode circulation

FIG. 10 Perturbation pressures (negative dotted) and winds for Ri 1000 warm core case (q_c = 0.49976; Ro = 0.849368; f = 4.0 $10^{-5} s^{-1}$); (a) lower layer; (b) upper layer. Y - direction distances are relative to center of the y domain.

The upper and lower perturbation velocity, pressure, and thickness fields for the Ri 1000 warm core case are shown in Figs. 10 and 11. The circulations are distinctly ageostrophic with convergence into the center of the lower layer low and divergence from the center of the upper layer high situated directly above the low. The positive (negative) meridional flow in the warm (cold) portions of the perturbation at the location of the lower layer low (high) corresponds to $W_{BCAG} > 0$ while the rising (sinking) motion in the warm (cold) portions of the perturbation corresponds to $W_K > 0$. The symmetry in amplitude between the warm core cyclone and cold core anticyclone on the right side of Fig. 10 is associated with the reversible latent heating. The magnitude of the evaporative cooling in the subsiding fluid of the cold core anticyclone is equal to the latent heating by condensation in the rising fluid of the warm core cyclone. Since it is not realistic for all the condensate to evaporate, the cold core anticyclone should be cooled less and be correspondingly weaker (e.g. Curry 1987) than the warm core cyclone.
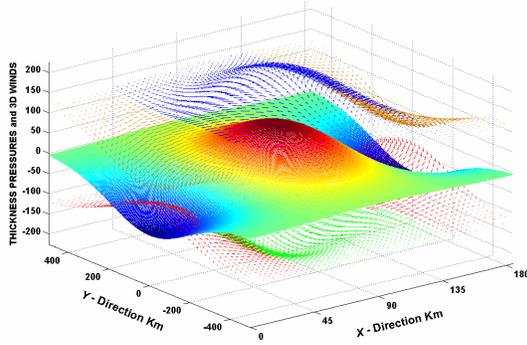
8

FIG. 11 Ri 1000 warm core case. Three dimensional perturbation winds projected on upper and lower layer perturbation pressure fields, respectively. Lower layer winds with positive (negative) vertical velocities: green (red). Upper layer winds with positive (negative) vertical velocities: blue (brown). Perturbation thickness field is colored mesh surface ranging from greatest red values to least blue values. *Y* - direction distances as in Fig. 10.

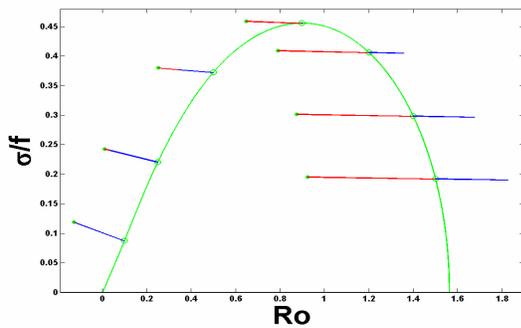### 3.5 Warm core mode sensitivity to scale

FIG. 12 Warm core as most unstable mode for Ri 40; q_c = 0.496; energy vectors and growth rates as in Fig. 9.

Fig. 12 shows the energy vectors varying as Ro increases for the Ri 40 warm core most unstable case (q_c = 0.496). For all Ro, $W_Q \gg W_{BC}$ as indicated by the energy vectors' rotation approaching 180°. As Ro increases beyond 0.899, its value for the preferred warm core scale, W_{BC} decreases toward large negative values as Ro approaches Ro$_{CUT}$ (1.562). This corresponds to the increasing down shear phase lag for Ro > 1 discussed above. In this case, the constraint on W_Q imposed by a fixed value of q_c combined with the decrease in perturbation thickness amplitude corresponding to the increased down shear phase lag (see Fig. 8d) stabilizes the mode for higher Ro. Similar behavior occurs for other values of Ri (not shown).

4. DISCUSSION

The primary motivation for this work has been to determine if there is an instability that can account for sub-synoptic scale, warm core, convergent circulations. To accomplish this, a two layer shallow water model on an *f*-plane has been modified to include the effects of latent heat in a non-convective basic state. Previous investigations into the effect of latent heat release on baroclinic instability using quasi-geostrophic models have not conclusively demonstrated the existence of sub-synoptic warm core instabilities with preferred scales because they cannot capture the effects of ageostrophic flows. The shallow water model's simplicity and versatility make it a suitable tool for finding such instabilities and determining their structure and sensitivity to baroclinity and saturation.

4.1 Findings

For near saturated adiabatic non-convective conditions and a modicum of baroclinity, warm core instability exists with a finite growth rate that is independent of vertical shear. This instability has a unique preferred scale and a convergent circulation. The preferred scale varies directly with the vertical shear and inversely with *f*. The growth rate of this instability is an order of magnitude larger while its scale is an order of magnitude less than in the corresponding dry case. All growth rates vary directly with *f*.

4.2 Comparison with quasi-geostrophic baroclinic instability

The warm core instability found in this study shares several characteristics with quasi-geostrophic baroclinic instability in a moist basic state. Both instabilities have reduced length scales and increased growth rates as the latent heating reduces the effective static stability toward the convective threshold. Once the convective threshold is reached, both instabilities have a maximum growth rate at the smallest scale. Moreover, both instabilities display increased upshear phase lag with height as latent heating increases. The distinction between the instabilities is the degree that these characteristics change with latent heating. This is particularly true of the upshear phase lag.

This distinction arises from the ageostrophic baroclinic energy conversion, W_{BCAG}, which is not available in quasi-geostrophic models. As baroclinity decreases, both quasi-geostrophic and the current ageostrophic treatment require the baroclinic conversion, W_{BC}, to make up the decreasing difference between adiabatic cooling, W_K, and latent heating, W_Q, as the convective threshold is approached. However, the quasi-geostrophic baroclinic instability requires a positive geostrophic baroclinic conversion, W_{BCG}, which constrains the unstable modes to have an upshear phase tilt with height. This constraint does not exist for the ageostrophic instability as W_{BCAG} permits warm core modes and even down shear tilted modes to be the

9

preferred unstable modes near the convective threshold. Moreover, the inapplicability of the quasi-geostrophic assumption at larger Ro is not an issue for the ageostrophic flows permitted in the shallow water model. Thus higher Ro solutions characterized by convergent flows are still valid. One caveat, however, is that the shallow water model is hydrostatic which implies that the horizontal scale $\gg$ vertical scale. This constrains the scales to be no smaller than sub-synoptic.

4.3 Most likely basic state conditions for instability

For the non-convective basic states used in this investigation, the baroclinity (vertical shear) required to produce warm core instability decreases toward zero as q_c approaches the saturated adiabatic value of 0.5, the convective threshold. Combining this with the direct relationship between shear strength and spatial scale discussed in the following sub-section, nearly saturated non-convective, low shear sub-synoptic regions appear to be favorable locations for the type of warm core instability found in the current investigation. Applying the finding by Nolan et al. (2007) that, for favorable surface vapor flux conditions in a zero shear environment, pre-existing circulations are catalysts for warm core cyclogenesis, the instability found here may generate such catalytic circulations on the appropriate sub-synoptic scale in a low shear, non-convective nearly saturated adiabatic environment.

4.4 Vertical shear strength, scale, and instability potential

Although the warm core instability found here has a growth rate independent of vertical shear strength, the preferred spatial scale is directly proportional to it. Thus, the probability of the atmosphere producing the required spatial scale of non-convective nearly saturated adiabatic conditions for a range of vertical shears must be considered. To the extent that it is more likely that somewhat spatially uniform, nearly saturated conditions exist over sub-synoptic rather than synoptic-scale areas, weaker vertical shears with their smaller L_{WC} should increase the likelihood of these instabilities because of the more frequent occurrence of smaller spatial scales of near saturation compared to larger ones.

Conversely, stronger vertical shears stabilize sub-synoptic regions whose moisture and stability characteristics might otherwise be spatially sufficient to destabilize sub-synoptic disturbances under weaker vertical shear conditions. This occurs because stronger vertical shears have larger values of L_{CUT}, which stabilize a broader range of warm core instabilities with $L_{WC} < L_{CUT}$. This is consistent with the finding of Kaplan and DeMaria (2003) that weak but non-zero vertical shears are nearly indistinguishable from zero shears in their effect on tropical cyclone intensification, whereas somewhat stronger shears markedly reduce the likelihood of intensification.

Davis and Bosart (2006) observe that vertical shear can play a dual and offsetting role in tropical cyclogenesis and intensification. On the one hand the synoptic scale lift from a preceding baroclinic disturbance can moisten the atmosphere and help spin up the lower tropospheric circulation. On the other hand vertical shear can tilt and displace the ensuing convection and thus inhibit intensification. While the current investigation does not address the role of convection in warm core mode development, it attempts to bridge the gap (e.g. Davis and Bosart 2006) between the synoptic scale of precursor disturbances and the sub-synoptic scale of developing warm core disturbances.

ACKNOWLEDGMENTS

APPENDIX

The Newton-Raphson Method of Solution

This technique follows IFW, except for the modifications to include latent heat release. IFW (3.9) becomes:

$$\overline{h}(1-q)\frac{d^2\hat{p}_1}{dy^2} + \frac{d\overline{h}}{dy}\frac{d\hat{p}_1}{dy} -$$

$$[k^2\overline{h}(1-q) + \frac{fk}{(\sigma + kU_1)}\frac{d\overline{h}}{dy}]\hat{p}_1$$

$$-\frac{\overline{\rho}}{(\rho_1 - \rho_2)g}[f^2 - (\sigma + kU_1)^2](\hat{p}_1 - \hat{p}_2) \quad (A1)$$

$$-(H - \overline{h})q\frac{(\sigma + kU_2)}{(\sigma + kU_1)}\frac{[f^2 - (\sigma + kU_1)^2]}{[f^2 - (\sigma + kU_2)^2]}$$

$$(k^2\hat{p}_2 - \frac{d^2\hat{p}_2}{dy^2}) = 0,$$

and IFW(3.10) becomes:

$$(\overline{h} - H)(1 - q)\frac{d^2\hat{p}_2}{dy^2} + \frac{d\overline{h}}{dy}\frac{d\hat{p}_2}{dy} -$$

$$[k^2(\overline{h} - H)(1 - q) + \frac{fk}{(\sigma + kU_2)}\frac{d\overline{h}}{dy}]\hat{p}_2$$

$$-\frac{\overline{\rho}}{(\rho_1 - \rho_2)g}[f^2 - (\sigma + kU_2)^2](\hat{p}_1 - \hat{p}_2) \qquad \text{(A2)}$$

$$+\overline{h}q\frac{(\sigma + kU_1)}{(\sigma + kU_2)}\frac{[f^2 - (\sigma + kU_2)^2]}{[f^2 - (\sigma + kU_1)^2]}$$

$$(k^2\hat{p}_1 - \frac{d^2\hat{p}_1}{dy^2}) = 0.$$

At $y = 0$, applying $\overline{h} = 0$ and IFW (3.17), eqn (A1) becomes:

$$\frac{d\overline{h}}{dy}\frac{d\hat{p}_1}{dy} - \frac{fk}{(\sigma + kU_1)}\frac{d\overline{h}}{dy}\hat{p}_1$$

$$-\frac{\overline{\rho}}{(\rho_1 - \rho_2)g}[f^2 - (\sigma + kU_1)^2](\hat{p}_1 - \hat{p}_2) \qquad \text{(A3)}$$

$$= 0,$$

and at $y = L_y$, applying $\overline{h} - H = 0$ and IFW (3.16), eqn (A2) becomes:

$$\frac{d\overline{h}}{dy}\frac{d\hat{p}_2}{dy} - \frac{fk}{(\sigma + kU_2)}\frac{d\overline{h}}{dy}\hat{p}_2$$

$$-\frac{\overline{\rho}}{(\rho_1 - \rho_2)g}[f^2 - (\sigma + kU_2)^2](\hat{p}_1 - \hat{p}_2) \qquad \text{(A4)}$$

$$= 0.$$

Following IFW (A.3) through IFW (A.13), boundary conditions eqn (A3) and IFW (3.17) at $y = 0$, with $\hat{p}_1\big|_{y=0} = D$ and $\hat{p}_2\big|_{y=0} = 1$, are integrated using eqn (A1) and eqn (A2) over a 5,000 interval grid to $y = L_y$. The errors in eqn (A4) and IFW (3.16) at $y = L_y$ determine corrections in σ and D. The integration iterates until the corrections in σ and D become arbitrarily small.

REFERENCES

Andrews, D. G., J. R. Holton, and C. B. Leovy, 1987: *Middle Atmospheric Dynamics.* Academic Press, 489 pp.

Arakawa, A., 2004: The cumulus parameterization problem: past, present, and future. *J. Climate,* **17,** 2493–2525.

Bannon, P. R., 1986: Linear development of quasi-geostrophic baroclinic disturbances with condensational heating. *J. Atmos. Sci.,* **43,** 2261–2274.

Charney, J. G., and A. Eliassen, 1964: On the growth of the hurricane depression. *J. Atmos. Sci.,* **21,** 68–75.

Craig, G. C., and S. L. Gray, 1996: CISK or WISHE as the mechanism for tropical cyclone intensification. *J. Atmos. Sci.,* **53,** 3528–3540.

Curry, J., 1987: The contribution of radiative cooling to the formation of cold-core anticyclones. *J. Atmos. Sci.,* **44,** 2575-2592.

Davis, C. A., and L. F. Bosart, 2006: The formation of hurricane Humberto (2001): the importance of extra-tropical precursors. *Quart. J. Roy. Meteor. Soc.,* **132,** 2055-2085.

Descamps L., D. Ricard, A. Joly, and P. Arbogast, 2007: Is a real cyclogenesis case explained by generalized linear baroclinic instability? *J. Atmos. Sci.,* 64, 4287–4308.

Emanuel, K. A., 1986: An air-sea interaction theory for tropical cyclones. Part I: Steady state maintenance. *J. Atmos. Sci.,* **43,** 585–604.

___, 1989: The finite-amplitude nature of tropical cyclogenesis. *J. Atmos. Sci.,* **46,** 3431–3456.

Fraedrich, K., and J. L. McBride, 1995: Large-scale convective instability revisited. *J. Atmos. Sci.,* **52,** 1914–1923.

Frank, W. M., and P. E. Roundy, 2006: The role of tropical waves in tropical cyclogenesis. *Mon. Wea. Rev.,* **134,** 2397–2417.

Holton, J. R. 2004: *An Introduction to Dynamic Meteorology.* 4th ed. Academic Press, 535 pp.

Houze, R. A., Jr., 2004: Mesoscale convective systems. *Rev. Geophys.,* **42,** RG4003.

Kaplan, J., and M. DeMaria, 2003: Large-scale characteristics of rapidly intensifying tropical cyclones in the North Atlantic basin. *Wea. Forecasting,* **18,** 1093-1108.

Majda, A. J., and M. G. Shefter, 2001: Waves and instabilities for model tropical convective parameterizations. *J. Atmos. Sci.,* **58,** 896-914.

Mak, M., 1981: An inquiry on the nature of CISK. Part I. *Tellus,* **33,** 531–537.

___, 1982: On moist quasi-geostrophic baroclinic instability. *J. Atmos. Sci.,* **39,** 2028–2037.

___, 1983: On moist quasi-geostrophic barotropic instability. *J. Atmos. Sci.,* **40,** 2349–2367.

McBride, J. L., and K. Fraedrich, 1995: CISK: a theory for the response of tropical convective complexes to variations in sea surface temperature. *Quart. J. Roy. Meteor. Soc.,* **121,** 783-796.

Mechoso, C. R., and D. M. Sinton, 1983: On the energy analysis of the two-layer frontal model. *J. Atmos. Sci.,* **40,** 2069–2074.

Montgomery, M. T., M. E. Nicholls, T. A. Cram, and A. B. Saunders, 2006: A vertical hot tower route to tropical cyclogenesis. *J. Atmos. Sci.,* **63,** 355-386.

Moorthi, S., and A. Arakawa, 1985: Baroclinic instability with cumulus heating. *J. Atmos. Sci.,* **42,** 2007–2031.

Nolan, D. S., E. D. Rappin, and K. A. Emanuel, 2007: Tropical cyclogenesis sensitivity to environmental parameters in radiative-convective equilibrium. *Quart. J. Roy. Meteor. Soc.,* 133, 2085–2107.

Orlanski, I., 1968: Instability of frontal waves. *J. Atmos. Sci.,* **25,** 178–200.

Simmons, A. J., 1974: The meridional scale of baroclinic waves. *J. Atmos. Sci.,* **31,** 1515–1525.

Sinton, D. M., 1984: Instability and nonlinear evolution of frontal waves. Ph.D. thesis., University of California, Los Angeles, 114 pp.

___, and C. R. Mechoso, 1984: Nonlinear evolution of frontal waves. *J. Atmos. Sci.,* **41,** 3501-3517.

___, and W. D. Heise, 1993: Frontal instability in a sheared basic state. *J. Atmos. Sci.,* **50,** 1691–1707.

Thorncroft, C. D., and B. J. Hoskins, 1990: Frontal Cyclogenesis. *J. Atmos. Sci.,* **47,** 2317–2336.

Thorpe, A. J., and K. A. Emanuel, 1985: Frontogenesis in the presence of small stability to slantwise convection. *J. Atmos. Sci.,* **42,** 1809–1824.

Tokioka, T., 1973: A stability study of medium-scale disturbances with inclusion of convective effects. *J. Meteor. Soc. Japan,* **51,** 1–9.

Wang, B., and A. Barcilon, 1986: Moist stability of a baroclinic zonal flow with conditionally unstable stratification. *J. Atmos. Sci.,* **43,** 705–719.

Xu, K.-M., and K. A. Emanuel, 1989: Is the tropical atmosphere conditionally unstable? *Mon. Wea. Rev.,* **117,** 1471-1479.